

## Studies of relaxation processes in $\text{BaF}_2:\text{La}^{3+}$ crystals by ionic-thermocurrent techniques

E. Laredo, M. Puma, and D. R. Figueroa

*Departamento de Física, Universidad Simón Bolívar, Apartado 80659, Caracas, Venezuela*

(Received 30 June 1978)

Ionic thermocurrent (ITC) experiments have been performed on  $\text{BaF}_2$  single crystals doped with  $\text{La}^{3+}$  with concentrations ranging from  $10^{-4}$  to  $10^{-2}$  (molar fractions). For crystals with a concentration lower than  $10^{-2}$ , the spectrum consists of three peaks, *A*, *B*, and *C*. For the most-doped crystal there is an additional peak attributed to polarizable clusters. To calculate the dipole concentrations from the depolarization curves, a new method is presented. Based on the results of thermal treatments and concentration-dependent studies, peaks *A* and *B* are assigned to nearest-neighbor and next-nearest-neighbor dipoles, respectively. The relaxation parameters are  $E_A = 0.39$  eV,  $\tau_0 = 4.9 \times 10^{-13}$  sec,  $E_B = 0.50$  eV, and  $\tau_0 = 3.4 \times 10^{-12}$  sec. The effect of thermal and mechanical treatments on the highest-temperature peak is studied. It is proposed that the dislocations present in the crystal are responsible for this relaxation.

### I. INTRODUCTION

When trivalent rare-earth ions ( $R^{3+}$ ) are introduced in crystals with the fluorite structure, it is known that the impurity goes in substitutionally. The  $R^{3+}$  substitutes a divalent alkaline-earth ion in the cation sublattice. The charge compensation is provided by an interstitial fluorine,  $\text{F}_i^-$ . This interstitial can be in the vicinity of the impurity ion, forming with it a dipole which can be oriented with an electric field. If the polarization state is frozen by lowering the temperature, then as the temperature increases in the absence of the electric field, the reorientation of these dipoles by thermally activated jumps will give rise to a depolarization current.<sup>1</sup> This current recorded in an ionic-thermocurrent (ITC) experiment contains information on the dipoles present in the crystal. Dielectric relaxation<sup>2</sup> together with ITC techniques<sup>3</sup> have been widely used recently to study the dipolar complexes present in fluorite structures. The experiments have been interpreted with the help of EPR results on the same systems when the impurity ions are paramagnetic. In this way, tetragonal sites, attributed to  $R^{3+} - \text{F}_i^-$  dipoles in nearest-neighbor (nn) position, and trigonal sites, attributed to  $R^{3+} - \text{F}_i^-$  dipoles in next-nearest-neighbor (nnn) position, have been identified in the fluorites. These two configurations are shown in Fig. 1.

In  $\text{CaF}_2$  crystals, lines assigned to impurities in cubic symmetry have also been observed. These lines have originated a recent controversy in the literature,<sup>4</sup> as the existence of non locally compensated cubic sites is not acceptable at such high concentrations. The cubic lines have been interpreted by Fong and co-authors,<sup>5</sup> for crystals under equilibrium growth conditions and with a concentration in the 0.01–0.5-mol% range, as

spatial averaging of dimeric clusters. Another interpretation by O'Hare and co-workers<sup>6</sup> is the existence of a local cubic phase.

In what concerns the local compensation, the predominant dipolar species depends mainly on the host matrix and the impurity ion size. In  $\text{CaF}_2$  the most frequent defect structure has a tetragonal symmetry, as has been seen by ESR experiments in the case of Ce,<sup>7</sup> Nd,<sup>8</sup> Gd,<sup>9</sup> Er,<sup>10</sup> and Yb.<sup>11</sup> The dielectric relaxation<sup>12</sup> and ITC studies<sup>13</sup> on  $\text{CaF}_2$  doped with all the elements of the lanthanide series have been interpreted in terms of nn dipoles and of several types of larger clusters.

The situation is somewhat different in the case of  $\text{SrF}_2$ , where, depending on the size of the impurity, the predominant dipoles are either the nn or nnn dipoles. A thorough ITC study of  $\text{SrF}_2$  doped with all the ions of the lanthanide series by Lenting *et al.*<sup>14</sup> shows that for  $R^{3+}$  from lanthanum to europium nn dipoles only exist, and from holmium to lutetium, dipoles assigned to nnn positions are the only ones detected. When the crystals are doped with ions of an intermediate size such as Gd, Tb, and Dy,  $\text{SrF}_2$  shows the presence of both types of dipoles. The study of the impurity

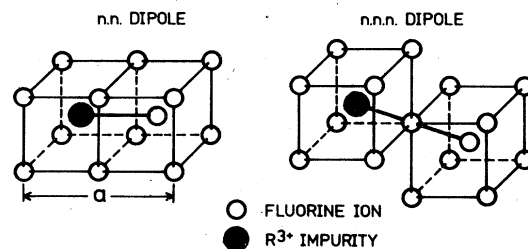


FIG. 1. The structure of nn and nnn dipolar complexes in  $\text{MF}_2:\text{R}^{3+}$ .

site symmetry by EPR experiments in the case of Ce,<sup>7</sup> Nd,<sup>8</sup> Gd, Tb, Dy,<sup>15</sup> and Yb,<sup>11</sup> confirms the validity of this assignment.

In  $\text{BaF}_2$  crystals, which have the largest lattice constant, the situation is again different. When  $\text{BaF}_2$  is doped with Gd (Refs. 9 and 15) or Yb (Ref. 11), a line with trigonal symmetry is found and attributed to nnn dipoles. In the case of  $\text{BaF}_2:\text{Ce}^{3+}$ , the predominant dipole is identified as nn.<sup>7</sup> The tetragonal line was, however, not found in the  $\text{BaF}_2:\text{Nd}^{3+}$  system.<sup>8</sup> Kitts *et al.*<sup>3</sup> have been able to identify a weak line with tetragonal symmetry in the EPR spectrum of  $\text{BaF}_2:\text{Gd}^{3+}$  in addition to the more intense line with trigonal symmetry. The ITC spectrum of these crystals consists of a broad line which can be separated into two components. The peak at 173 K is attributed to nn dipoles, while the peak at 193 K is due to nnn dipoles. The latter kind of dipoles are ten times more abundant than the nn dipoles.

Lanthanum is the largest rare-earth ion with an ionic radius of 1.32 Å,<sup>16</sup> but it is not a suitable impurity for ESR studies. However, due to its lack of paramagnetism, it has been used as a dopant in  $\text{BaF}_2$  to study fluorine diffusion by nuclear-magnetic-resonance techniques.<sup>17</sup>

ITC experiments on  $\text{BaF}_2:\text{La}^{3+}$  would yield information on the defect structure of this system which has not been investigated before. Because of the lack of information about the site symmetries, it will be necessary to perform thermal treatments and concentration-dependence experiments in order to identify the relaxation processes responsible for the different ITC peaks.

## II. THEORY

The model<sup>1</sup> used to interpret ITC experimental results is based on the assumption of noninteracting dipoles with electric moment  $\mu$  and concentration  $N/\text{cm}^3$ . These dipoles reorient by thermally activated jumps of the  $\text{F}_i^-$  around the impurity ions. The jumps are characterized by a relaxation time  $\tau(T)$ :

$$\tau(T) = \tau_0 \exp(E/kT), \quad (1)$$

where  $\tau_0$  is the reciprocal frequency factor and  $E$  is the activation energy involved in the reorientation process.

The current density  $J(T)$ , due to the reorientation of the dipoles, is

$$J(T) = -b \frac{dP(T)}{dT} = \frac{P(T)}{\tau(T)}, \quad (2)$$

where  $b$  is the linear heating rate and  $P(T)$  is the remanent polarization of the sample at the temperature  $T$ . After an integration of relation (2), it is found that the polarization  $P(T)$  can be ex-

pressed as

$$P(T) = P_0 \exp \left( -\frac{1}{b\tau_0} \int_{T_f}^T \exp(-E/kT') dT' \right), \quad (3)$$

where  $P_0$  is the saturation polarization at the polarization temperature  $T_p$  and  $T_f$  is the temperature at which the applied electric field  $E_p$  is switched off. The temperature  $T_f$  is chosen in such a way that the typical times involved in the experiments are very small compared to  $\tau(T_f)$ . In the case of a cubic crystal,  $P_0$  can be written

$$P_0 = N\mu^2 E_p / 3kT_p, \quad (4)$$

where it is assumed that  $kT_p \gg \mu E_p$  and the field  $E_p$  has been applied during a time  $t_p \gg \tau(T_p)$ .

The expression for the current density is found by using relations (2) and (3):

$$J(T) = \frac{P_0}{\tau_0} \exp(-E/kT) \times \exp \left( -\frac{1}{b\tau_0} \int_{T_f}^T \exp(-E/kT') dT' \right). \quad (5)$$

The saturation polarization  $P_0$  can be calculated from the area under the curve of  $J(T)$  vs  $T$ .  $P_0$  can also be evaluated, from the knowledge of the activation energy  $E$  and the maximum current density  $J(T_M)$  occurring at a temperature  $T_M$ , in the following way. Let us take the derivative of the current density with respect to the temperature which yields

$$\frac{1}{J(T)} \frac{dJ(T)}{dT} - \frac{E}{KT^2} = -\frac{1}{b\tau_0} \exp(-E/kT). \quad (6)$$

Combining relations (6) and (2), the expression for  $P(T)$  is

$$P(T) = \frac{1}{b} \frac{J(T)}{E/kT^2 - [1/J(T)] [dJ(T)/dT]}. \quad (7)$$

$P(T_M)$ , the remanent polarization at the temperature  $T_M$ , can be written

$$P(T_M) = \frac{1}{b} \frac{J(T_M)}{E/kT_M^2}. \quad (8)$$

On the other hand, the ratio  $P(T_M)/P_0$  can be expressed as a function of  $E/kT_M$ . From expression (3),  $P(T)$  can be written

$$P(T) = P_0 \exp f(T), \quad (9)$$

where

$$f(T) = -\frac{1}{b\tau_0} \int_0^T \exp(-E/kT') dT'. \quad (10)$$

In relation (10) the lower limit of the integral has been taken as zero without any consequence to the value of  $f(T)$ .

Defining a new variable  $\xi$  as  $\xi \equiv E/kT$  and per-

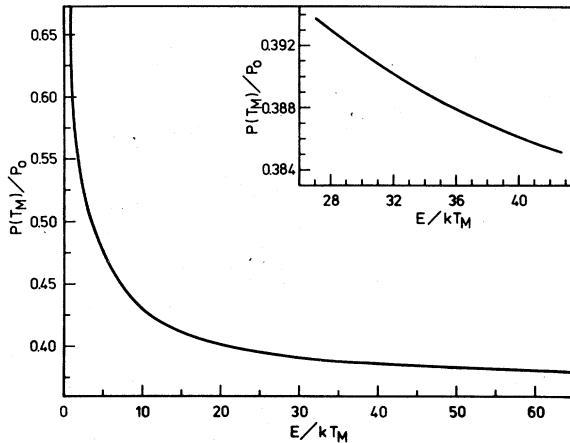


FIG. 2. Variation of the ratio  $P(T_M)/P_0$  as a function of  $E/kT_M$ . The inset shows an expanded region of the plot for the most frequent values of  $E/kT_M$ .

forming an integration by parts, the integral in expression (10) yields

$$f(\xi) = -\xi_M^2 \exp(\xi_M) \left( \frac{\exp(-\xi)}{\xi} - \int_{\xi}^{\infty} \frac{\exp(-\xi')}{\xi'} d\xi' \right), \quad (11)$$

where  $\xi_M \equiv E/kT_M$  and  $E/kb\tau_0 = \xi_M^2 \exp(\xi_M)$ . This last equality can be deduced easily from expression (6) by setting the derivative  $dJ(T)/dT$  equal to zero at  $T = T_M$ . The exponential integral in expression (10) can be evaluated from its rational approximation<sup>18</sup> valid for  $1 \leq \xi < \infty$ . The value of the function  $f(\xi)$  for  $\xi = \xi_M$  is

$$f(\xi_M) = -\xi_M \left( 1 - \frac{\xi_M^2 + a_1 \xi_M + a_2}{\xi_M^2 + b_1 \xi_M + b_2} \right),$$

with

$$a_1 = 2.334733, \quad b_1 = 3.330657$$

$$a_2 = 0.250621, \quad b_2 = 1.681534.$$

Once  $f(\xi_M)$  is known,  $P(T_M)/P_0$  can be computed. In Fig. 2 a plot of  $P(T_M)/P_0$  vs  $E/kT_M$  is shown. The typical values of  $E/kT_M$  found in an ITC spectrum range from 30 to 40, approximately. This region of the plot is represented in greater detail in the inset of Fig. 2.

In conclusion, it has been shown that with the knowledge of  $E$ ,  $J(T_M)$ , and  $T_M$ , the saturation polarization  $P_0$  can be obtained without having to estimate the area under the curve  $J(T)$  vs  $T$ .

### III. EXPERIMENTAL PROCEDURE

The samples are  $\text{BaF}_2$  single crystals with an area of  $1 \text{ cm}^2$  and a thickness of  $1 \text{ mm}$ . The nominal amount of  $\text{La}^{3+}$  doping ranges from  $10^{-4}$  to  $10^{-2}$  in molar fractions. The faces of the crystals

are not painted or coated with any conductive material.

The crystal slab is held in the ITC cell by two vertical plates connected by thin walled stainless-steel tubes to the cell teflon cover. The cell is first evacuated to a pressure of  $1 \times 10^{-6}$  Torr or less, then filled with pure dry nitrogen for the duration of the polarization and cooling of the crystal. The static electric field  $E_p$  used for the polarization of the sample at a temperature  $T_p$  ranges from 10 to 20 kV/cm; the polarization time  $t_p$  is about 3 min. The sample is then cooled from  $T_p$  to  $T_f$ , where the dipole relaxation time  $\tau(T_f)$  is estimated to be very long compared to any time interval involved in the experiment. The electric field is then switched off and the cell evacuated and filled with pure dry helium at a pressure of 100 Torr. The temperature is then increased from 77 K to 400 K at a linear rate  $b$ , typically  $b \approx 0.1 \text{ K sec}^{-1}$ . The current emitted by the crystal, due to its depolarization, is detected by a vibrating reed electrometer, Cary 401M. This signal is recorded versus temperature on an X-Y recorder. The increasing temperature is also registered versus time in order to measure the heating rate provided by a temperature controller. The temperature sensor is a copper-constantan thermocouple in thermal contact with one of the electrodes, but electrically insulated from it. Our detection system has a sensitivity of  $10^{-16}$  A and the results are reproducible within 3%.

Thermal treatments, such as annealings at high temperature, were done in a quartz tube filled with dry helium. The temperature was lowered at a rate of  $10 \text{ K h}^{-1}$ . Quenchings were also performed, after keeping the crystal at high temperature for 4 h in dry helium, by removing the quartz tube from the furnace and cooling it to room temperature in about 3 min.

### IV. RESULTS

The ITC spectrum observed for an as-given  $\text{BaF}_2$  crystal doped with  $5 \times 10^{-4} \text{ La}^{3+}$  is shown in Fig. 3. It consists of three peaks, A, B, and C, with the maxima depolarization currents occurring at temperatures  $T_{MA} = 141 \text{ K}$ ,  $T_{MB} = 194 \text{ K}$ , and  $T_{MC} = 287 \text{ K}$ , respectively. This spectrum is very similar to the one obtained for all the as-given crystals up to a concentration of  $5 \times 10^{-3}$ . For the crystal with the highest nominal concentration ( $10^{-2}$ ), the spectrum is more complicated, as can be seen in Fig. 4. After cleaning peaks A and B for several crystals, by partial discharge, the relaxation parameters have been determined from the current on the low-temperature side of the depolarization peak. The corresponding

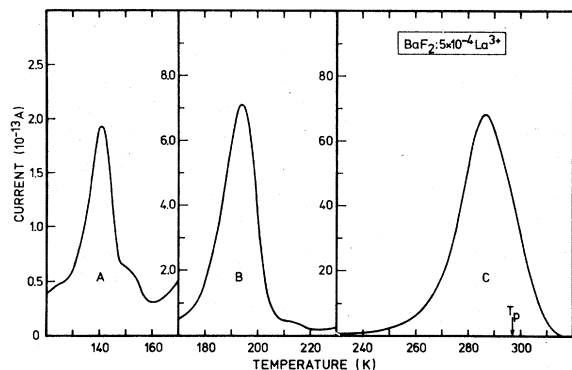


FIG. 3. ITC spectrum for an as-given crystal of  $\text{BaF}_2:\text{La}^{3+}$  with a nominal concentration of  $5 \times 10^{-4}$  (molar fraction).

values of the activation energy  $E$  and the relaxation time  $\tau_0$  are  $E_A = 0.39 \pm 0.02$  eV,  $\tau_{0A} = 4.9 \times 10^{-13 \pm 0.7}$  sec,  $E_B = 0.50 \pm 0.02$  eV,  $\tau_{0B} = 3.4 \times 10^{-12 \pm 0.5}$  sec. We have not used the area method in the determination of these parameters because the peaks are somewhat broadened on the high-temperature side for all the concentrations reported here. As will be discussed in Sec. V, we have attributed the small  $A$  peak to nn dipole reorientation and peak  $B$  to nnn dipole relaxation. We exclude the possibility that peaks  $A$  and  $B$  are due to large clusters, as they exist at the lowest concentration reported here ( $10^{-4}$ ). Moreover, the ratio of the intensities of the maxima  $H_A/H_B$  is constant and equal to 0.24 for the whole concentration range. To calculate the dipole concentration responsible for each depolarization peak, the method generally used is to measure the area under the current curve. These areas under the ITC peak are in our case somewhat enhanced for peak  $A$  by the existence

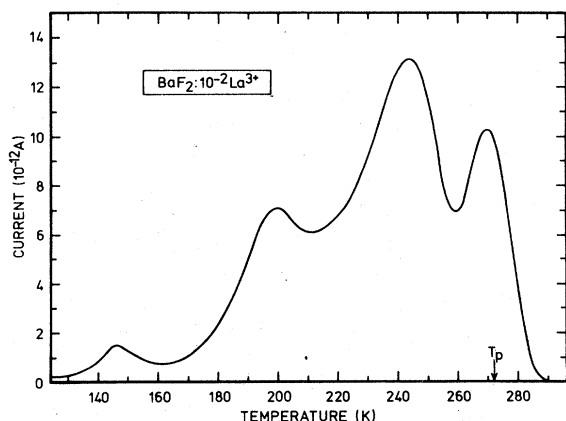


FIG. 4. ITC spectrum for an as-given crystal of  $\text{BaF}_2:\text{La}^{3+}$  with a nominal concentration of  $10^{-2}$  (molar fraction).

of a weak relaxation on the high-temperature side and for peak  $B$  by the presence of the strong high-temperature  $C$  peak which contributes to the tail of the curve. We have, therefore, used the result found in Sec. II to calculate the total number of dipoles of each type given the energy  $E$ , temperature  $T_M$ , and height  $J(T_M)$  of the maximum, heating rate  $b$ , polarization temperature  $T_P$ , and field  $E_p$ . We calculate first  $\xi_M$  and find from Fig. 2 the corresponding  $P(T_M)/P_0$ . Then  $P(T_M)$  is evaluated from relation (8), knowing the maximum current density. From expression (4) the dipole concentration  $N_A$  or  $N_B$  is calculated, assuming an unrelaxed point ion model for the calculation of the dipole moments. In Fig. 5 the variation of the dipole concentration versus the nominal impurity concentration is plotted for each kind of dipole. The ratio  $N_A/N_B$  is constant, and the total impurity concentration in dipolar form, that is,  $N_A + N_B$ , is always less than the nominal impurity concentration  $c$ . For the less doped crystals,  $N_A + N_B$  is close to  $c$ ; however, the ratio  $(N_A + N_B)/c$  decreases strongly for concentrations greater than  $10^{-3}$ .

Several thermal treatments were made in order to confirm the origin of peaks  $A$  and  $B$ . Crystals quenched from high temperature (1250 K) showed a spectrum qualitatively similar to the as-given crystals in what concerns peaks  $A$  and  $B$ . However, the intensity of these peaks is slightly greater than that for the as-given crystals, but the ratio  $H_A/H_B$  is still conserved. On the other hand, annealings at high temperatures (1250 K), in which the temperature was lowered

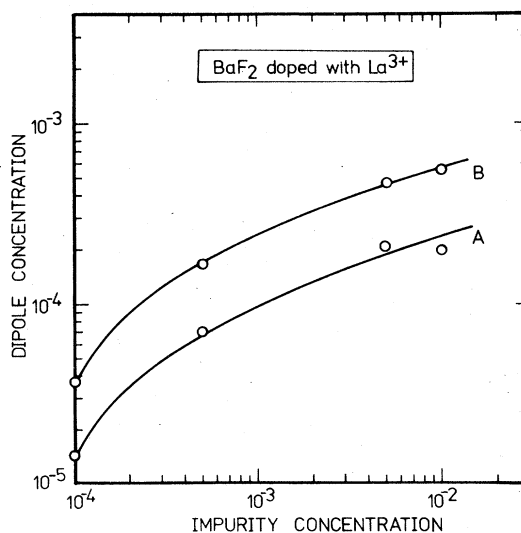


FIG. 5. The total concentration of nn dipoles (peak  $A$ ) and nnn dipoles (peak  $B$ ) is represented as a function of the nominal impurity content in  $\text{BaF}_2:\text{La}^{3+}$  crystals.

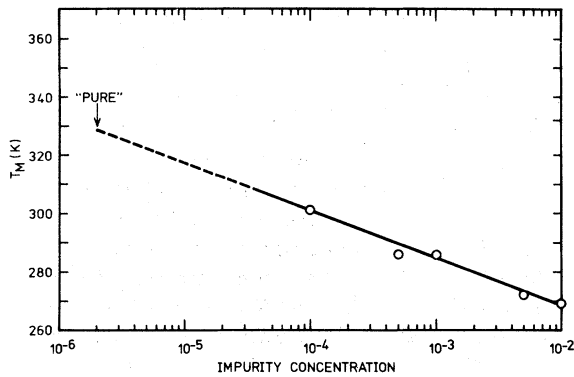


FIG. 6. Temperature dependence of the maximum of peak C as a function of the impurity concentration in  $\text{BaF}_2:\text{La}^{3+}$ .

at a very slow rate ( $10 \text{ K h}^{-1}$ ), erased from the spectra all traces of peaks A and B. A subsequent quenching from the same high temperature restores the initial intensities for peaks A and B.

For the heavily doped crystals ( $c = 10^{-2}$ ), the behavior is again different. An additional peak located at 244 K, the most intense peak of the spectrum shown in Fig. 4, disappears completely after quenching, while the intensity of peak C increases.

Let us now concentrate on the behavior of peak C in the less-doped crystals ( $c < 10^{-2}$ ). In the as-given crystals, the most intense signal was always located at high temperature. The intensity of peak C was always at least ten times higher than the intensity of peak B. The concentration dependence of the height  $H_c$  of this signal was studied, and the height of the peak varied consid-

erably with the concentration but not in a monotonic way. Several attempts to measure an activation energy did not yield a unique value. Energies obtained from the as-given crystals ranged from 0.85 to 0.65 eV as  $c$  increased. Furthermore, for similar heating rates and polarization temperatures, the current maximum occurred at a temperature  $T_{MC}$  which varied with the concentration of  $\text{La}^{3+}$ . In Fig. 6 we have plotted the variation of  $T_{MC}$  vs  $c$  for as-given crystals polarized at room temperature. As one can see in Fig. 6, when the number of defects increases, the position of the current maximum drifts to lower temperatures, going from 301 K for the less-doped crystal to 270 K for the highest concentration. In order to understand this anomalous behavior, the crystals were thermally treated. First the samples were annealed at high temperature and cooled to room temperature very slowly. The change in the position of the maximum of peak C was drastic. Peak C, compared to the as-given crystal, appeared translated to higher temperatures. This shift was about 40 K in the case of the crystals with a concentration  $c = 10^{-3}$  and  $5 \times 10^{-3}$ . Then the crystals were quenched from 1250 K. Compared to the as-given crystals, the effect of the quenching on the height of the peak was strong, but it did not change the position of the maximum which was almost restored to its initial value. In other words, the peak shifted back to lower temperatures in going from the annealed to the quenched samples.

In one of the quenched crystals ( $c = 5 \times 10^{-3}$ ), a mechanical stress was then applied to bend the sample. This stress was intense enough to break it in two halves. The ITC spectrum obtained

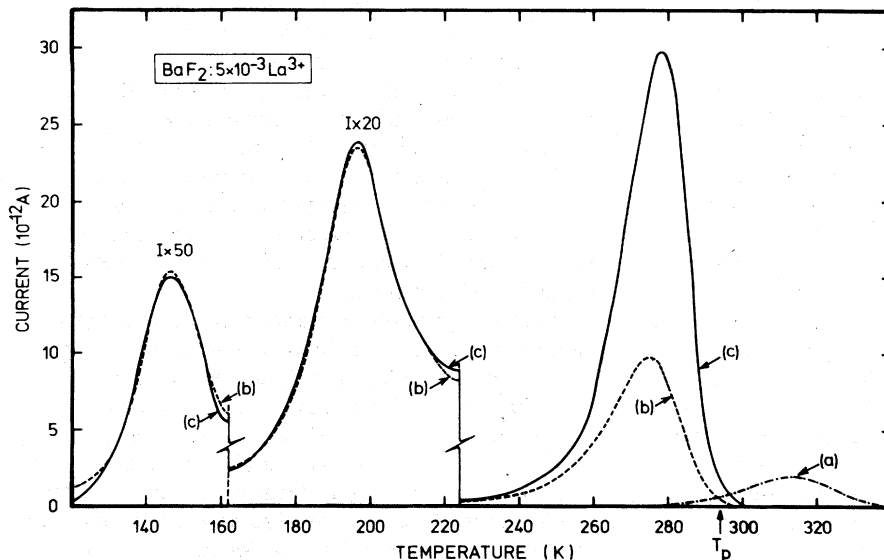


FIG. 7. ITC spectra for  $\text{BaF}_2:5 \times 10^{-3}$ -mole %  $\text{La}^{3+}$  after several treatments: (a) annealed at 1250 K, (b) quenched from 1250 K, (c) mechanically stressed. The intensities of the two lowest-temperature peaks have been magnified by the factors shown.

from one of these halves showed a *C* peak with an intensity higher than that produced by the whole quenched crystal with its maximum located at the same temperature. However, the intensity of peaks *A* and *B* decreased according to the reduction of the crystal area. In Fig. 7, all the results described above are summarized for a sample with  $5 \times 10^{-3}$  impurity concentration. In order to take into account the two different sizes of the crystals studied, the appropriate correction factor was used in drawing curve 7(c). It is worth mentioning that the other half of the crystal gave a spectrum which showed the same features.

### V. DISCUSSION

In  $\text{BaF}_2$  crystals it is generally accepted that both types of dipoles coexist; it is also believed that nnn dipoles are more abundant than nn dipoles. The energies involved in the reorientation of nnn dipoles should be nearer to the value of the migration energy of the free interstitial anions than the energies necessary for the reorientation of the more tightly bound nn dipoles. The migration energy for the free  $\text{F}_i^-$  is 0.76 eV, as has been measured by ionic conductivity and NMR relaxation techniques<sup>17</sup> on the same samples used in this work. Another cause for the existence of an ITC peak may be the presence of large reorientable clusters with a net dipolar moment. For low doping concentrations ( $c < 10^{-3}$ ), the presence of clusters is not expected in fluorite crystals as the interstitial aggregation is unimportant.<sup>19</sup> Therefore, if we start from dilute crystals, as the impurity concentration increases, we expect the number of each type of dipoles to grow faster than for higher concentration when cluster formation is likely. Furthermore, the dependence of the number of dipoles versus concentration should be the same for both types.

If we focus our attention on the behavior of peaks *A* and *B* for the as-given  $\text{BaF}_2$  crystals reported in Sec. IV, it is found that in line with the preceding argument and with the results shown in Fig. 5, we can identify the dipoles responsible for peak *A* as nn ( $E_A = 0.39$  eV) and for peak *B* as nnn ( $E_B = 0.50$  eV). The behavior of the quenched crystals confirms this assignment, as the only change observed is a slight increase in the intensity of peaks *A* and *B*, but their ratio was preserved. The question arises as from where the extra amount of dipoles comes. When the crystals were annealed, peaks *A* and *B* disappeared, as can be seen in Fig. 7(a) for a crystal with a concentration of  $5 \times 10^{-3}$ . This indicates that in  $\text{BaF}_2:\text{La}^{3+}$  some kind of complexes that cannot be oriented with an electric field are formed at the ex-

pense of the dipoles. These complexes exist even at low concentrations. A subsequent quenching of these crystals prevents the aggregation of the dipoles, as seen in Fig. 7(b). In  $\text{BaF}_2:\text{La}^{3+}$  it should be noticed that the presence of nn and nnn dipoles depends strongly on the thermal history of the samples, and a low concentration alone does not seem to exclude the presence of aggregates. Besides, in this system polarizable clusters seem also to exist for the highest concentration ( $c = 10^{-2}$ ). The peak located at  $T_M = 244$  K in Fig. 4 is not appreciable for lower concentrations and disappears after quenching the sample. This peak is probably due to some kind of polarizable clusters.

Due to its reported behavior, peak *C* cannot be assigned either to dipole or cluster relaxation. The accumulated evidence on its behavior indicates that it can be attributed to a relaxation process related to the dislocations present in the crystal.

It is a well-known fact that the mechanical stress applied on a crystal increases its dislocation density. In Fig. 7 the differences observed between curves (b) and (c) are the exclusive result of the crystal deformation. In consequence, the increase in the dislocation density can be thought to be directly responsible for the enhancement of the *C* peak intensity. This fact can also be checked by observing the changes in the *C* peak between an as-given and a quenched crystal. In the latter case the intensities are always higher and the position of the *C* peak is not significantly shifted. In a crystal containing immobile impurities, as is the case in  $\text{BaF}_2:\text{La}^{3+}$ , the impurities act as pinning points for the dislocations. One of the meaningful parameters of a dislocation is the free average length between pinning points,  $\lambda$ . As the impurity concentration increases, the average distance between impurity cations decreases. In Fig. 6 the temperature of the maximum for peak *C* is seen to increase when the concentration is lowered. A nominally pure crystal has also been studied after annealing. It shows a *C* peak located at 328 K which would yield an impurity concentration of 2 ppm under extrapolation of the straight line shown in Fig. 6, which is a reasonable estimate for the background impurity concentration of the "pure" crystal.

One of the possible explanations, or at least a useful visualization of the process, is to consider the dislocation charged with an average free length  $\lambda$  and surrounded by a charge cloud.<sup>20</sup> Any displacement of the dislocation with respect to its charge cloud will originate an electric dipole. The restoring force on the dislocation lines,<sup>21</sup> besides its electrostatic part, has also an elastic contribution related to  $\lambda$ . As the free length decreases,

the elastic contribution to the restoring force increases. The average free length  $\lambda$  can be varied by the introduction of impurities in the lattice. When  $\lambda$  is short the relaxation of the displaced dislocation is easier than in the case of a less-doped crystal with a longer  $\lambda$ . Therefore, the dislocation with shorter  $\lambda$  will relax at lower temperatures than the dislocation with longer  $\lambda$ .

A crystal with such dislocations will give an ITC signal due to the relaxation of the dislocations with respect to their charge clouds. This peak should be broad because of the distribution of values of  $\lambda$  around its average, and should be located at temperatures which increase as  $c$  decreases. Besides, for a given  $\lambda$  its intensity should be proportional to the dislocation density of the crystal. This is the observed behavior of peak  $C$  as can be seen in Figs. 6 and 7. Assigning the origin of peak  $C$  to dislocation relaxation, the

position of the maximum gives an indication of the value of  $\lambda$ .

In conclusion, peak  $C$  can give an estimate of the amount of impurities acting as pinning centers for dislocations in  $\text{BaF}_2:R^{3+}$  crystals. The contribution of dislocations to the ITC spectrum has not been mentioned before, as far as we know, and if quantitatively explained, could yield a better understanding of the relaxation processes present in the fluorite structures.

#### ACKNOWLEDGMENTS

This work was partly supported by the Consejo Nacional de Investigaciones Científicas y Tecnológicas de Venezuela (CONICIT), and we wish to express our gratitude to them. The authors also thank Dr. Alan Chadwick of the University of Kent at Canterbury for providing most of the crystals used in this work.

<sup>1</sup>C. Bucci, R. Fieschi, and G. Guidi, *Phys. Rev.* **148**, 816 (1966).

<sup>2</sup>J. Fontanella and C. Andeen, *J. Phys. C* **9**, 1055 (1976).

<sup>3</sup>E. L. Kitts, Jr., M. Ikeya, and J. H. Crawford, Jr., *Phys. Rev. B* **8**, 5840 (1973).

<sup>4</sup>E. Secemski and W. Low, *J. Chem. Phys.* **64**, 4240 (1976).

<sup>5</sup>F. K. Fong, *J. Chem. Phys.* **61**, 1604 (1974).

<sup>6</sup>J. M. O'Hare, T. P. Graham, and G. T. Johnston, *J. Chem. Phys.* **61**, 1602 (1974).

<sup>7</sup>A. Kiel and W. B. Mims, *Phys. Rev. B* **6**, 34 (1972).

<sup>8</sup>A. Kiel and W. B. Mims, *Phys. Rev. B* **7**, 2917 (1973).

<sup>9</sup>Chi-Chung Yang, Sook Lee, and A. J. Bevolo, *Phys. Rev. B* **13**, 2762 (1976).

<sup>10</sup>U. Ranon and W. Low, *Phys. Rev.* **132**, 1609 (1963).

<sup>11</sup>U. Ranon and A. Yaniv, *Phys. Lett.* **9**, 17 (1964).

<sup>12</sup>C. Andeen, D. Link, and J. Fontanella, *Phys. Rev. B*

**16**, 3762 (1977).

<sup>13</sup>E. L. Kitts, Jr. and J. H. Crawford, Jr., *Phys. Rev. B* **9**, 5264 (1974).

<sup>14</sup>B. P. M. Lenting, J. A. J. Numan, E. J. Bijvank, and H. W. den Hartog, *Phys. Rev. B* **14**, 1811 (1976).

<sup>15</sup>J. Sierro, *Phys. Lett.* **4**, 178 (1963).

<sup>16</sup>R. D. Shannon and C. T. Prewitt, *Acta Crystallogr. B* **25**, 925 (1969).

<sup>17</sup>D. R. Figueroa, A. V. Chadwick, and J. H. Strange, *J. Phys. C* **11**, 55 (1978).

<sup>18</sup>*Handbook of Mathematical Functions*, edited by M. Abramowitz and I. Stegun (Dover, New York, 1965), p. 231.

<sup>19</sup>C. R. A. Catlow, *J. Phys. C* **9**, 1845 (1976).

<sup>20</sup>A. B. Lidiard, *Crystals with the Fluorite Structure*, edited by W. Hayes (Clarendon, Oxford, 1974).

<sup>21</sup>R. W. Whitworth, *Adv. Phys.* **24**, 203 (1976).